The EMBO Journal Vol. 19 No. 17 pp. 4838–4845, 2000

Structure of the ArsA ATPase: the catalytic subunit of a heavy metal resistance pump

Tongqing Zhou, Sergei Radaev, Barry P.Rosen and Domenico L.Gatti[1]

Department of Biochemistry and Molecular Biology, Wayne State University School of Medicine, 540 E. Canfield Avenue, Detroit, MI 48201, USA

[1]Corresponding author
e-mail: mimo@david.med.wayne.edu

Active extrusion is a common mechanism underlying detoxification of heavy metals, drugs and antibiotics in bacteria, protozoa and mammals. In *Escherichia coli*, the ArsAB pump provides resistance to arsenite and antimonite. This pump consists of a soluble ATPase (ArsA) and a membrane channel (ArsB). ArsA contains two nucleotide-binding sites (NBSs) and a binding site for arsenic or antimony. Binding of metalloids stimulates ATPase activity. The crystal structure of ArsA reveals that both NBSs and the metal-binding site are located at the interface between two homologous domains. A short stretch of residues connecting the metal-binding site to the NBSs provides a signal transduction pathway that conveys information on metal occupancy to the ATP hydrolysis sites. Based on these structural features, we propose that the metal-binding site is involved directly in the process of vectorial translocation of arsenite or antimonite across the membrane. The relative positions of the NBS and the inferred mechanism of allosteric activation of ArsA provide a useful model for the interaction of the catalytic domains in other transport ATPases.

Keywords: antimonite/ArsA/arsenite/protein structure/resistance

Introduction

All organisms, whether archaea, prokaryotes or eukaryotes, have evolved mechanisms of resistance to toxic xenobiotics (Dey and Rosen, 1995). Life emerged in waters that were probably rich in ionic metals, and thus it is likely that resistance to these compounds pre-dated the evolution of drug resistance (Rosen, 1999). In *Escherichia coli*, high-level resistance to arsenite and antimonite is conferred by the *ars* operon of plasmid R773 (Silver *et al*., 1981). The *arsA* and *arsB* genes of the operon encode, respectively, the catalytic subunit (ATPase) and the membrane subunit of a pump that extrudes arsenite and antimonite ions from the cytosol (Chen *et al*., 1986). When expressed in the absence of ArsB, ArsA can be isolated as a soluble ATPase that displays a 15- to 20-fold enhancement of activity upon binding Sb(III) (Hsu and Rosen, 1989; Rosen *et al*., 1999). ArsA is composed of two homologous domains (>20% identity), designated A1 and A2, connected by a short linker (Chen *et al*., 1986; Li and Rosen, 2000). Each domain contains a consensus sequence for a nucleotide-binding site (NBS), and both NBSs are required for ATPase activity and antimonite transport (Karkaria *et al*., 1990; Kaur and Rosen, 1993). ArsA has long been recognized as a member of a superfamily of ATPases with diverse functions (Chen *et al*., 1986; Koonin, 1993; Zhou and Rosen, 1997), one of which is as the catalytic subunit of the ArsAB resistance pump. In both its structure and function, the ArsAB pump shows similarity to ABC transporters such as the human multidrug resistance P-glycoprotein (Gottesman *et al*., 1996; Ambudkar *et al*., 1999). Both ArsAB and P-glycoprotein are ATPases activated by the substrates they pump, both have two similar consensus NBSs and both have 12 membrane-spanning α-helices. The mechanism by which drugs activate the efflux pumps that confer resistance to those drugs is a major unanswered question in the field of resistance.

Here we present the crystal structure of the *E.coli* ArsA ATPase. Key features of the structure are two distinct NBSs, each composed of residues from both the A1 and A2 halves of the protein, a novel metalloid-binding site that allosterically modulates the ATPase activity and two signal transduction elements that physically connect the allosteric and catalytic sites.

Results

Overall structure

The structure of ArsA was determined by the multiwavelength anomalous diffraction (MAD) of a selenomethionine derivative and refined at 2.3 Å to an *R*-factor (R_{free}) of 20.7 (26.2) (Table I). The asymmetric unit of the crystal contains a single molecule of the entire ArsA (A1 + A2) with 46% solvent content. As predicted from the amino acid sequence similarity between the first and second half of the protein, ArsA consists of two structurally homologous domains (r.m.s. deviation between A1 and A2 of 1.6 Å for 187 C_αs; Figure 1A). Each domain is approximately L-shaped, with a core of one antiparallel and seven parallel strands with helices on both sides of the central sheet (Figure 1B). This topology is a variation of the typical Rossmann fold observed in many other nucleotide-binding proteins. The two arms of each L-shaped domain overlap the structurally equivalent regions of the other domain to form a diamond shaped molecule with a central cavity (Figures 1A and 2). A pseudo-2-fold axis of symmetry oriented along one of the diamond diagonals establishes the relative position of the two domains. If this axis is aligned vertically, a horizontal plane coincident with the other diagonal of the diamond divides the molecule into a lower half containing the NBSs and an upper half containing the metal-binding site (Figure 1A).

Table I. Data collection and refinement statistics

	Native (30–2.3 Å)	Se-Met (30–2.5 Å)		
Data collection				
Wavelength (Å)	1.5418	0.9788	0.9785	0.9500
Measurements	178 456	396 445	400 113	566 664
Unique reflections	27 783	42 104	42 176	42 403
<Redundancy>	6.4	9.4	9.5	13.4
Completeness[a] (%)	98.2 (91.4)	96.7 (77.7)	96.8 (79.2)	97.3 (84.1)
$\langle I\rangle/\sigma\langle I\rangle$	18.8 (2.5)	38.7 (6.6)	35.7 (5.4)	39.3 (6.9)
R_{merge}[b] (%)	8.6	6.0	6.3	6.1
Phasing statistics				
Mean figure of merit			0.71 (0.44)	
R_{Cullis}[c] (disp) (%)		0.56 (0.85)	0.70 (0.91)	
R_{Cullis} (ano) (%)		0.41 (0.73)	0.43 (0.76)	0.59 (0.83)
Phasing power[d] (disp)		2.20 (0.85)	1.33 (0.55)	
Phasing power (ano)		4.00 (1.50)	3.92 (1.44)	2.39 (1.06)
Refinement statistics (30–2.3 Å, no σ cut-off)				
R_{cryst}[e] (%)	20.7			
R_{free} (%)	26.2			
Amino acids	586			
Water molecules	223			
$\langle B\rangle$ (Å^2) protein	49.6			
$\langle B\rangle$ (Å^2) waters	51.3			
R.m.s.d. bond lengths (Å)	0.011			
R.m.s.d. bond angles (°)	1.8			
R.m.s.d. impropers (°)	1.35			
φΨ angles (%)				
most favored	91.1			
allowed	8.7			

Friedel mates were counted as independent reflections in the Se-Met data set.
[a]Values in parentheses refer to the highest resolution bin (0.1 Å wide).
[b]$R_{merge} = \sum_h\sum_i|I(h)_i - \langle I(h)\rangle|/\sum_h\sum_i I(h)_i$, where $I(h)_i$ is the ith measurement.
[c]R_{Cullis} = r.m.s.(E)/r.m.s.(ΔF), where E is the phase-integrated lack of closure and ΔF is the dispersive (disp) or anomalous (ano) difference.
[d]Phasing power = r.m.s.(F_H)/r.m.s.(E), where F_H is the calculated heavy-atom structure factor.
[e]$R_{cryst} = \sum||F_{obs} - F_{calc}|/\sum|F_{obs}|$. R_{free} was calculated on 10% of the data omitted from refinement.
Stereochemistry was assessed with PROCHECK (CCP4, 1994).

The nucleotide-binding sites

Many ATPases, including ABC transporters, have duplicated consensus sequences indicative of the presence of two distinct NBSs (Ambudkar *et al*., 1999). However, it is not clear from the primary sequence of these proteins whether each catalytic site is contained entirely within a single domain or whether it requires contributions from more than one domain. The structure of ArsA shows that, at least in this enzyme, the NBSs are formed by residues from both halves of the protein (Figures 1A and 2). The two NBSs are located at the interface between the A1 and the A2 domains and in close proximity to each other such that the α carbons of the two P-loops are only 8 Å apart at their closest approach. The surface of one NBS is contributed mostly by residues of the A1 domain, with a smaller contribution from the A2 domain: we refer to this site as the A1 NBS (Figure 2, left panel). The surface of the second NBS is contributed mostly by residues of the A2 domain with a smaller contribution from the A1 domain: we refer to this site as the A2 NBS (Figure 2, right panel).

ArsA crystallizes in the presence of Sb(III) and Mg-ADP (Zhou *et al*., 1999), and crystals are stable in the presence of these ligands. Under these conditions, Mg-ADP occupies both NBSs (Figures 1 and 2). The phosphate groups of ADP bind to the GKGGVGKT sequence of the P-loop in the A1 or A2 domain. In both sites, Mg^{2+} is coordinated octahedrally (Figure 3). Mg ligands at the A1 NBS include the β-phosphate of ADP, three molecules of water, the hydroxyl of Thr22 and the carboxylate of Asp45. Coordination of Mg^{2+} in ATP- and GTP-binding proteins frequently involves an aspartic acid residue (Walker *et al*., 1982; Georgiadis *et al*., 1992; Harmark *et al*., 1992; Schindelin *et al*., 1997; Sprang, 1997; Larsen *et al*., 1998; Weber *et al*., 1998). Asp45 has been recognized previously as being essential for the ATPase activity; cells producing mutant ArsA proteins in which Asp45 is replaced by glutamate, asparagine or alanine have reduced resistance to arsenite (Zhou and Rosen, 1999). In addition, the purified D45E protein has decreased affinity for Mg^{2+}. Mg ligands at the A2 NBS include the β-phosphate of ADP, four water molecules and the hydroxyl of Thr341 (Figure 3). The latter occupies the equivalent position of Thr22 at the A1 NBS. Asp364, equivalent to Asp45 of the A1 NBS, is hydrogen bonded to one of the water molecules that directly coordinate the ion. This situation is reminiscent of the similar indirect coordination of Mg^{2+} by an aspartic acid residue via a water molecule observed in p21-RAS (Harmark *et al*.,

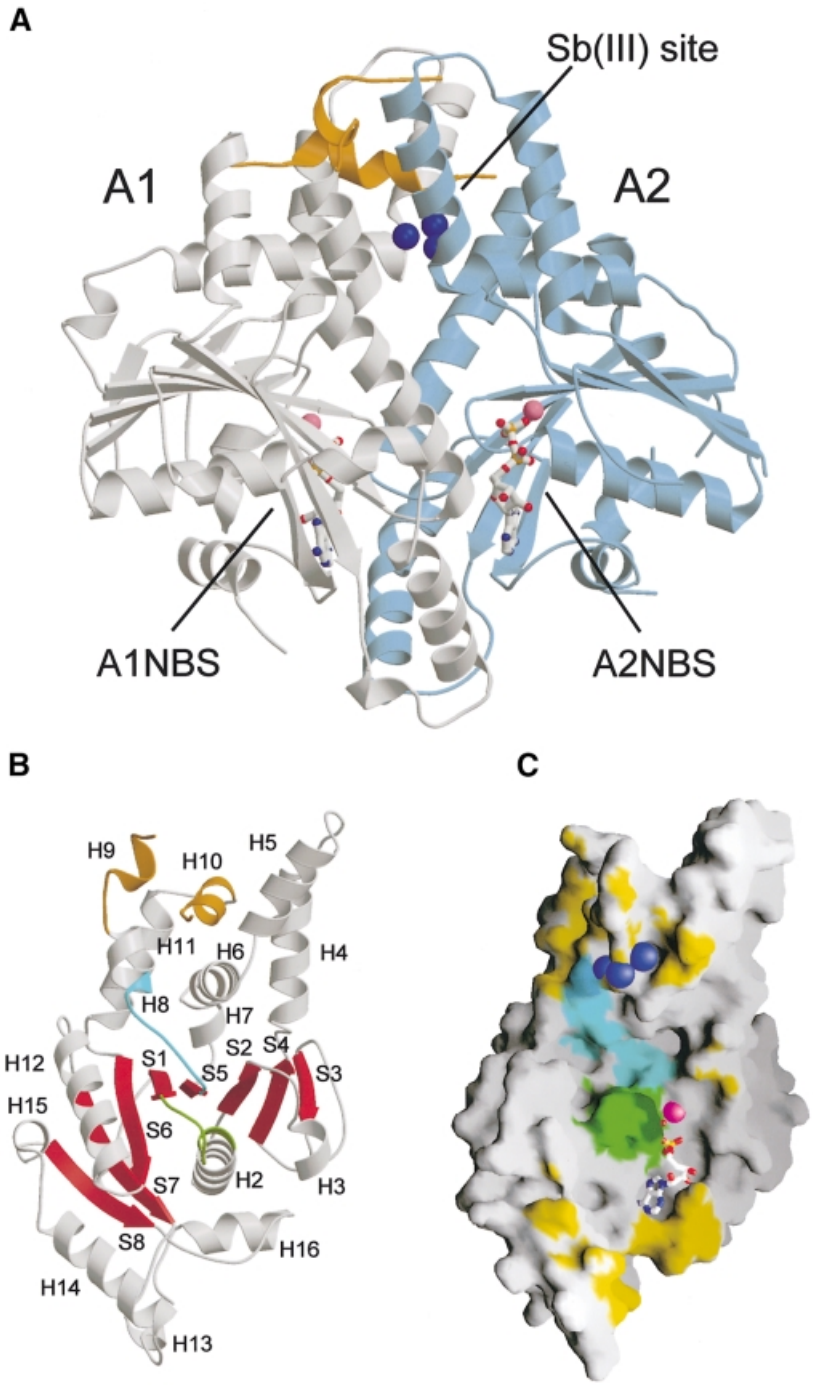

Fig. 1. (**A**) Overall structure of the ArsA ATPase. A front view of the enzyme is shown looking down the central cavity along a direction perpendicular to the pseudo-2-fold axis of symmetry that relates the A1 and A2 domains. The secondary structure elements are drawn as ribbon diagrams. A1 is colored in ivory, A2 in sky blue; helices H9–H10 of A1, which seal the antimony-binding site from above, are colored in orange. The equivalent helices of A2 are disordered and are not visible in the structure. Bound Sb(III) and Mg^{2+} are shown as space-filling models, and colored in blue and hot pink, respectively. ADP bound in the two NBSs is shown with ball-and-stick and colored according to atom type (phosphorus, yellow; oxygen, red; nitrogen, blue). (**B**) Structure of the A1 domain, viewed from the side that interacts with the A2 domain [this is equivalent to a rotation by 90° with respect to the view of the A1 domain shown in (A)]. The central core of eight strands is colored in red, and helices H9 and H10 are colored in orange as in (A). The P-loop and the DTAPTGH sequence (see text for details) are colored in chartreuse and cyan, respectively. The structure of the A2 domain is essentially identical to that of the A1 domain. (**C**) Molecular surface of the A1 domain viewed from the same angle as in (B). The P-loop and the DTAPTGH sequence are colored in chartreuse and cyan, respectively, as in (B). Regions of the molecular surface of the A1 domain that are <1.4 Å from the molecular surface of the A2 domain are highlighted in yellow or dark green (for the component of the P-loop), or in dark cyan (for the component of the DTAPTGH sequence). Bound Sb(III) and Mg^{2+} are shown as space-filling models, and colored in blue and hot pink, respectively. ADP bound in the A1 NBS is shown with ball-and-stick and colored according to atom type (phosphorus, yellow; oxygen, red; nitrogen, blue). H, helix; S, strand. Generated with MOLSCRIPT (Kraulis, 1991), RASTER3D (Merritt and Murphy, 1994) and GRASP (Nichols *et al*., 1991).

1992). Asp142 at the A1 NBS and Asp447 at the A2 NBS are also coordinated indirectly to Mg^{2+} through water molecules (Figure 3). These two aspartic acid residues are located at the N-terminal end of an elongated stretch of

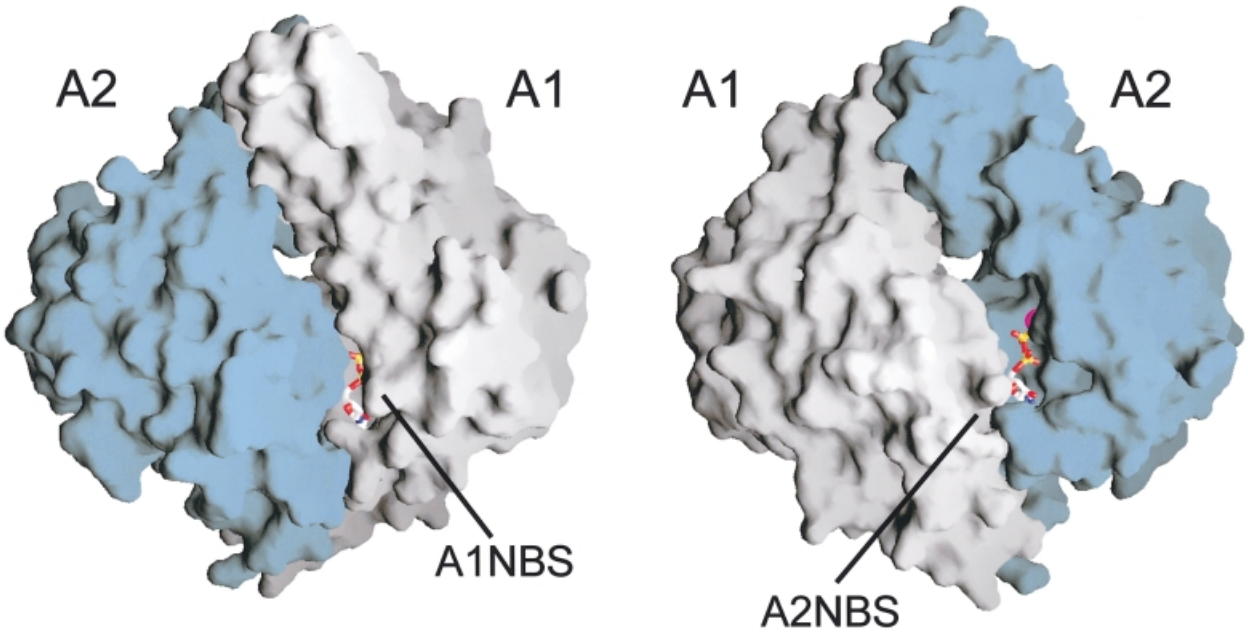

Fig. 2. The nucleotide-binding sites of ArsA. Two views of the molecular surface of ArsA show the relative positions of the A1 and A2 domains, and details of ADP bound in the A1 NBS (left image) and in the A2 NBS (right image). The A2 NBS appears more accessible than the A1 NBS. Generated with GRASP (Nichols *et al*., 1991).

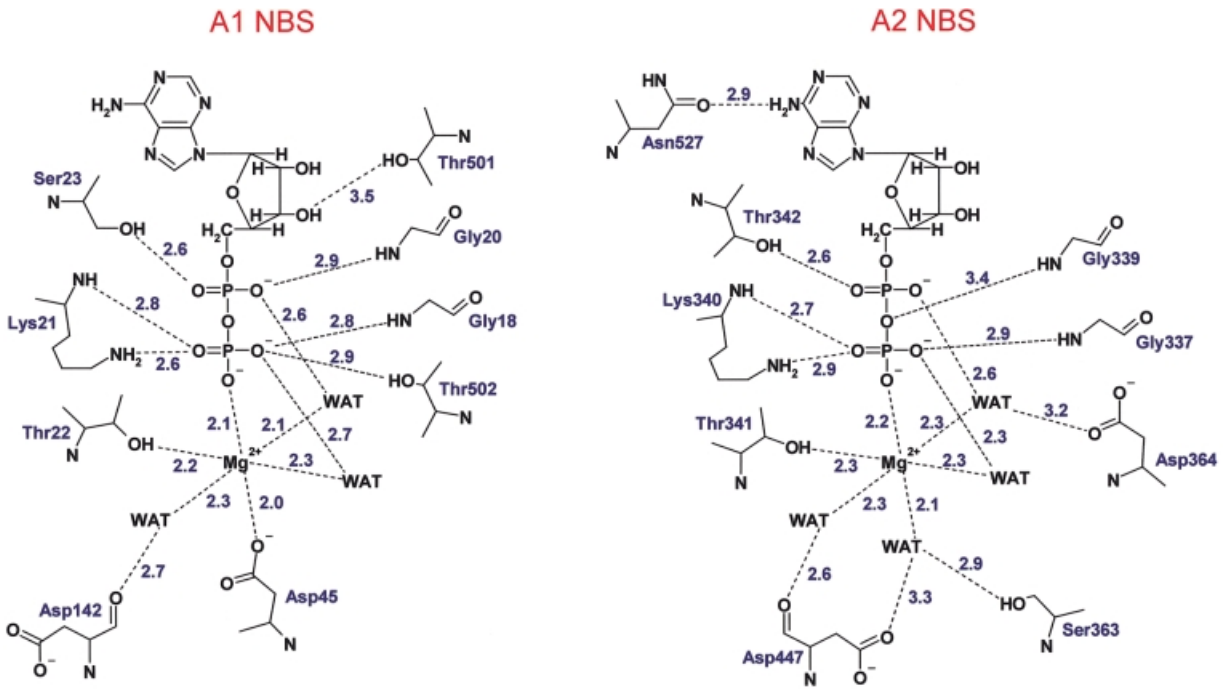

Fig. 3. Polar contacts of Mg-ADP at the A1 and A2 NBS. The octahedral coordination of Mg^{2+} is clearly evident. Asp142 and Asp447, representing the N-terminal ends of the signal transduction pathways, interact with Mg-ADP via water molecules. The 'closed' conformation of the A1 site is reflected by the presence of some short range interactions of the adenine nucleotide with residues of the A2 domain (see text for details). Distances are expressed in angstroms.

residues that extends from each NBS to the allosteric metal-binding site, and may be the primary effector of signal transduction between these centers (see below).

As previously mentioned, the adenine nucleotides bound at the two NBSs are stabilized by both polar and hydrophobic interactions reaching across the A1–A2 interface. For example, the hydroxyls of Thr501 and Thr502 from A2 form hydrogen bonds, respectively, with the ribose 3′-OH and with a β-phosphate oxygen of the ADP bound in the A1 NBS. However, Ser210 of the A2 NBS, equivalent to Thr502 of the A1 NBS, is >6 Å away from the β-phosphate of ADP. This difference reflects the fact that the A2 NBS appears to be in an 'open' conformation and is therefore much more accessible than the A1 NBS (Figure 2). The functional relevance of this observation is confirmed by experiments in which ArsA

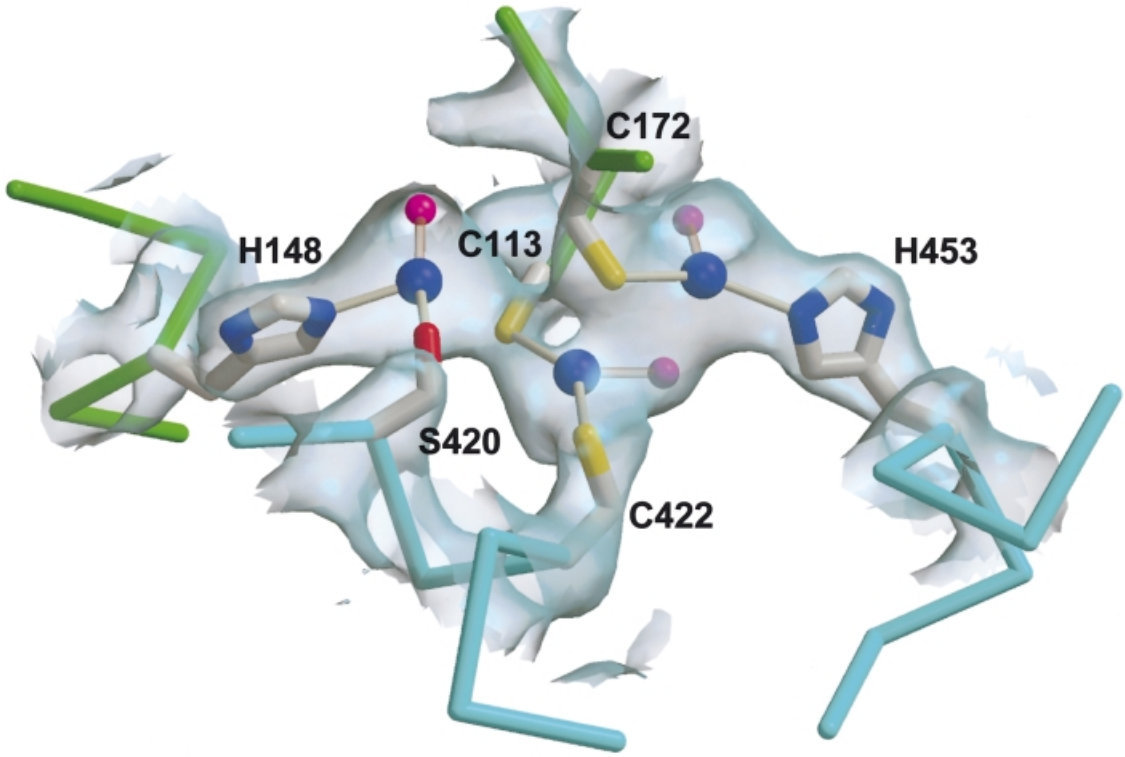

Fig. 4. The allosteric site of ArsA. An electron density map of the metal-binding site of ArsA is shown with a section of the refined model. The map, calculated with the amplitudes of the native data set and MAD phases improved with density modification and extended to 2.3 Å, is displayed as a transparent surface contoured at 1.2σ. Each antimony is coordinated by one residue from the A1 half, one residue from the A2 half and a non-protein ligand (most probably chloride). Antimony and chloride are shown as space-filling models and colored in dark blue and magenta, respectively. The A1 backbone is colored in chartreuse, the A2 backbone in cyan. Generated with BOBSCRIPT (Esnouf, 1997) and RASTER3D (Merritt and Murphy, 1994).

crystals were soaked in a holding solution containing the non-hydrolyzable ATP analog AMP-PNP (not shown). Under these conditions, it is possible to exchange the nucleotide at the A2 site, but not at the A1 site. These experiments are consistent with earlier studies suggesting that the A1 is a high affinity, poorly exchangeable site, while the A2 is a low affinity, easily exchangeable site (Kaur, 1999). The observed enzyme asymmetry may reflect inherent functional differences between the two NBSs or may be a consequence of the crystal lattice having frozen the enzyme in one step of the catalytic cycle.

The metal-binding site

The ArsA ATPase is allosterically regulated by its substrate metalloids As(III) and Sb(III). This is similar to the allosteric activation of the P-glycoprotein by drug substrates (Dey *et al*., 1998). The allosteric site of ArsA is located at the opposite end of the molecule with respect to the NBSs. Here the upper arms of the L-shaped domains cross to delimit a dome-shaped region of space overlooking the central cavity of the enzyme and containing a metal cluster with unusual characteristics. In this region, helices H4 and H5 of the A1 and A2 domain form two protuberances projecting outwards away from each other. The region of space in between them is occupied by helices H9 and H10 from the A1 domain (Figure 1A). The equivalent helices of the A2 domain are significantly more disordered and appear to point away from the region of space delimited by the two protuberances. Thus, structural elements from the A1 domain alone provide a ceiling to the metal center, whose sides are delimited by helix H6 from both domains. Three globular masses are present in the MAD-phased electron density map of this region (Figure 4), and also in an anomalous difference Fourier map (not shown), suggesting that the areas of high electron density correspond to three antimony atoms bound in the allosteric site. The metal ligands cannot be assigned unambiguously at the current resolution, but on the basis of the most likely coordination geometry it appears that each Sb(III) is bound to two residues: one Sb(III) to His148 (A1) and Ser420 (A2), one to Cys113 (A1) and Cys422 (A2), and one to Cys172 (A1) and His453 (A2). Additional density is visible in close proximity to each Sb(III) and may represent a third non-protein ligand of the metal (Figure 4). Modeling of these ligands as hydroxyl ions leaves residual positive densities in a difference Fourier map. The residual density is removed completely by modeling the additional ligands as chloride ions. Thus, each Sb(III) appears to be three-coordinate, with one ligand being a residue of the A1 domain, a second ligand being a residue of the A2 domain and possibly chloride as the third ligand. Overall, this pattern of coordination confirms earlier suggestions that the binding of the metal brings together the two domains of the enzyme, resulting in activation (Bhattacharjee *et al*., 1995; Bhattacharjee and Rosen, 1996; Rosen *et al*., 1999). Mutation of codons for His148 and His453 to alanine codons results in a 5-fold reduction in the rate of metal-stimulated ATP hydrolysis

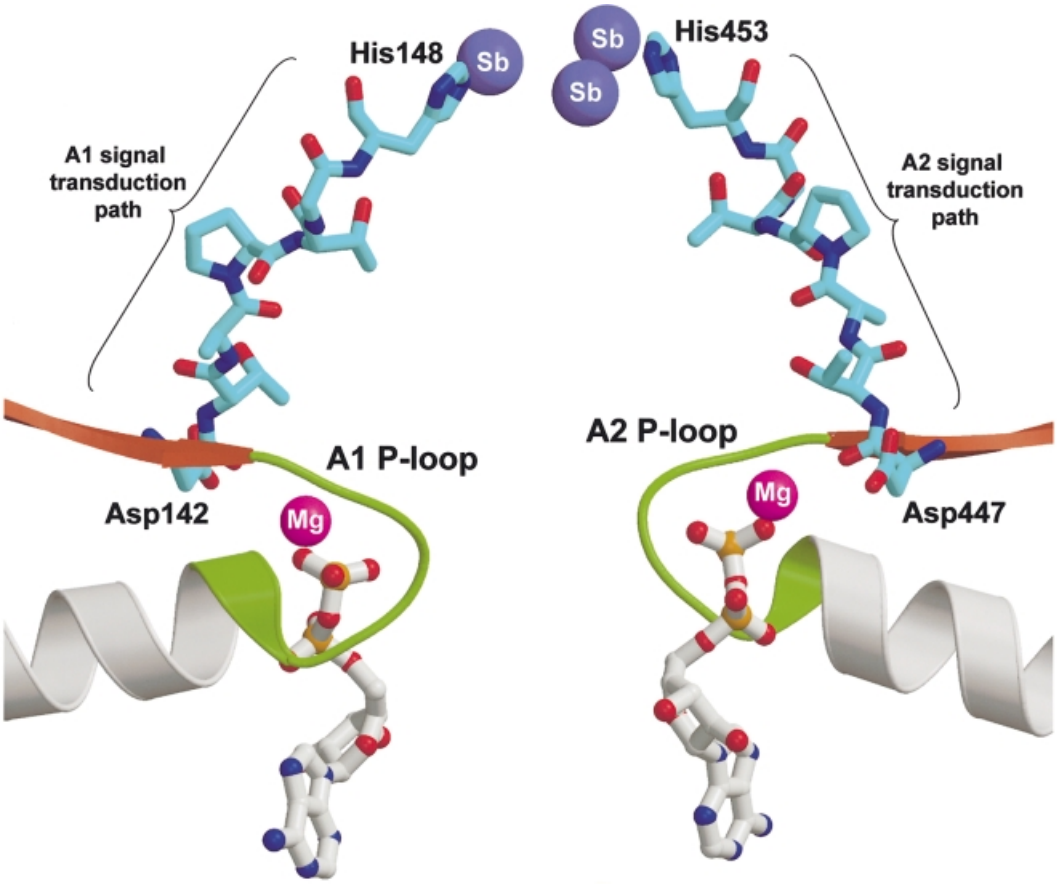

Fig. 5. The signal transduction pathway. Two stretches of seven residues with the identical sequence $D_{142/447}TAPTGH_{148/453}$ connect the A1 and A2 NBS to the metal-binding site. Strands (dark orange), helices (ivory) and P-loops (chartreuse) are drawn as ribbons. The nucleotides bound in the two NBSs are shown as ball-and-stick models colored according to atom type (phosphorus, yellow; oxygen, red; nitrogen, blue). The DTAPTGH sequences are shown as stick models with cyan bonds. Sb(III) (blue) and Mg^{2+} (hot pink) are shown as space-filling models. Generated with MOLSCRIPT (Kraulis, 1991) and RASTER3D (Merritt and Murphy, 1994).

(H.Bhattacharjee and B.P.Rosen, unpublished), whereas mutations of the cysteine ligands are significantly more severe. Mutation of the codons for Cys113, Cys172 or Cys422 to serine codons reduces resistance to background levels, indicating that these altered proteins have lost the ability to catalyze efflux (Bhattacharjee *et al*., 1995). Consistent with the effect of the mutations *in vivo*, purified C113S and C172S proteins exhibit a 20-fold increase in the concentration of antimonite required for half-maximal activation, and the C422S protein exhibits a 200-fold increase.

An additional binding site for antimonite was recognized in proximity to the adenine moiety of ADP at the A1 NBS. In this pocket, the hydrated form of an antimonite ion ($H_2SbO_3^-$) can be fitted in the electron density (not shown), and appears to be stabilized by a salt bridge to the guanidinium moiety of Arg206. However, the low occupancy of this ion (<0.5) and the fact that Arg206 is not conserved in other bacterial homologs of ArsA suggest that this secondary binding site for antimonite may not be of functional relevance.

The signal transduction path

The catalytic and allosteric sites are located distant from each other in the enzyme, requiring a mechanism to transmit the information of metal occupancy to the ATP hydrolysis site. Thus, it is of particular relevance that the two histidine ligands of the metal cluster (His148 and His453) are located at the C-terminal ends of two elongated stretches of residues that extend from the A1 and A2 NBSs to the metal-binding site (Figures 1B and C, and 5). The amino acid sequences of these segments, $D_{142/447}TAPTGH_{148/453}$, corresponding to the switch II region of other nucleotide-binding proteins (Georgiadis *et al*., 1992; Sprang, 1997; Schlessman *et al*., 1998), are identical in the A1 and A2 domains and are also invariant in ArsA homologs from yeast to humans (Zhou and Rosen, 1997; Rosen *et al*., 1999). The aspartic acid residues at the N-terminal ends of these sequences (Asp142 in A1 and Asp447 in the A2 domain) are in close proximity to the phosphate chain of the adenine nucleotide; in particular, Mg^{2+} at the A1 NBS is coordinated by a water molecule that forms a hydrogen bond with the backbone carbonyl of Asp142, and Mg^{2+} at the A2 NBS is coordinated by a water molecule that forms hydrogen bonds with both the backbone and the carboxylate of Asp447 (Figure 3). Other residues located on the carboxyl side of His148 or His453 are also engaged in a complex network of both van der Waals and polar interactions surrounding the metal cluster. These interactions may contribute signifi-

cantly to the strength of the signal conveyed from the metal-binding site to the NBS.

Discussion

Possibly the most interesting characteristic of the ArsA ATPase is the fact that it is activated by the binding of arsenite or antimonite, the same ions that are transported by the ArsAB pump. At this point, there is no conclusive structural or biochemical evidence that the ions which activate the hydrolytic activity of ArsA are the same ions that are transported across the membrane. However, it is tempting to suggest that a change in the affinity of ArsA for antimonite associated with ATP binding and hydrolysis at the NBSs might drive the vectorial uptake of antimonite from one side of the enzyme and its subsequent release at the interface with the ArsB moiety of the pump. In this context, it is of interest that the buried surface between the A1 and A2 domains is relatively small (<10%) compared with the total surface of the enzyme, such that ArsA is essentially a hollow protein with a large central cavity (Figure 1A and C). The metal-binding site is open below to this central cavity, and it is sealed above by the loop between helices H9 and H10 that provides the ligand Cys172. Thus, it is possible that during the catalytic cycle of ArsA, antimonite ions may access the metal site from the central cavity to then be injected into ArsB in association with a conformational change in the H9–H10 region. Vectorial transport would be assured by the concentration gradient across the membrane.

ArsA also presents several characteristics in common with the multidrug resistance P-glycoprotein of eukaryotic cells. Like ArsA, P-glycoprotein consists of two homologous halves separated by a linker (Ambudkar *et al*., 1999), and each half has an NBS whose function is tightly linked to that of the other half of the molecule (Senior *et al*., 1998; Hrycyna *et al*., 1999). Although there is limited sequence homology between ArsA and the nucleotide-binding domain of ABC transporters, a superposition of the A1 or A2 domain of ArsA on the catalytic subunit HisP of the histidine permease (Hung *et al*., 1998) shows that many elements of the structural core are oriented similarly. Based on crystal symmetry, a structure for the HisP dimer, and for the catalytic domain of ABC transporters in general, has been proposed in which the two NBSs are facing away from each other (Hung *et al*., 1998). It is not clear, however, how these two distant NBSs might interact and show strong catalytic cooperativity, a feature that, for example, has been clearly observed in the P-glycoprotein (Senior *et al*., 1998; Hrycyna *et al*., 1999). It is possible that the model proposed for the HisP dimer might be biased by the particular symmetry contacts present in the crystals of that protein. Such potential artifacts do not apply to the *E.coli* ArsA ATPase, which is a dimer of two monomers/domains that are part of the same polypeptide. Moreover, ArsA homologs purified from yeast and mouse are true dimers of a subunit equivalent in size to one of the two domains of the *E.coli* ArsA (H.Bhattacharjee, J.Shen and B.P.Rosen, unpublished). Thus, the specific mode of interaction between ArsA domains and the mechanism of allosteric activation by As(III)/Sb(III) in this protein provide a reasonable model for the way in which the nucleotide-binding domains of ABC transporters might interact to form a functional dimer and for the way in which these carriers are activated by their transported substrates.

Materials and methods

Crystals of *E.coli* ArsA (sg I222; a = 73.34, b = 75.64, c = 223.42 Å) were obtained as described by Zhou *et al*. (1999). The ArsA structure was determined using the MAD of a selenomethionine derivative. A MAD data set was collected at beamline X12C (NSLS, Brookhaven National Laboratories) at the selenium absorption edge and peak and at a remote wavelength using a charged couple device as detector (Table I). Oscillation data were processed with DENZO and SCALEPACK (Otwinowski and Minor, 1997). The positions of 11 out of 13 selenium atoms in the asymmetric unit were determined with SOLVE (Terwilliger and Berendzen, 1999). MAD phasing in the resolution range 30–2.5 Å was performed with CNS (Brünger *et al*., 1998). Phase improvement by means of density modification resulted in an electron density map of extremely high quality, and all the ordered region of the protein was traced easily using O (Jones *et al*., 1991). The structure was refined with CNS in the resolution range 30–2.3 Å (Table I) using cross-validated maximum likelihood as the target function (Adams *et al*., 1997) against a native data set collected with in-house equipment. The correctness of the model was assessed with the program DDQ (van den Akker and Hol, 1999). The current model (4469 atoms) consists of residues 1–296, 309–369, 378–461, 480–586, 223 water molecules, two Mg-ADP, three Sb(III), three Cl^-, one $H_2SbO_3^-$ and six Cd^{2+} ions. Coordinates have been deposited at the Protein Data Bank (accession code 1F48).

Acknowledgements

We thank Dr R.Sweet and the staff at beamline X12C (NSLS) for assistance with data collection, and Dr S.Ackerman for helpful discussions and critical reading of the manuscript. This work was supported by US Public Health Service grants GM55425 to B.P.R and AI43918 to D.L.G.

References

Adams,P.D., Pannu,N.S., Read,R.J. and Brünger,A.T. (1997) Cross-validated maximum likelihood enhances crystallographic simulated annealing refinement. *Proc. Natl Acad. Sci. USA*, **94**, 5018–5023.

Ambudkar,S.V., Dey,S., Hrycyna,C.A., Ramachandra,M., Pastan,I. and Gottesman,M.M. (1999) Biochemical, cellular and pharmacological aspects of the multidrug transporter. *Annu. Rev. Pharmacol. Toxicol.*, **39**, 361–398.

Bhattacharjee,H. and Rosen,B.P. (1996) Spatial proximity of Cys113, Cys172 and Cys422 in the metalloactivation domain of the ArsA ATPase. *J. Biol. Chem.*, **271**, 24465–24470.

Bhattacharjee,H., Li,J., Ksenzenko,M.Y. and Rosen,B.P. (1995) Role of cysteinyl residues in metalloactivation of the oxyanion-translocating ArsA ATPase. *J. Biol. Chem.*, **270**, 11245–11250.

Brünger,A.T. *et al*. (1998) Crystallography and NMR system: a new software suite for macromolecular structure determination. *Acta Crystallogr. D*, **54**, 905–921.

Chen,C.M., Misra,T.K., Silver,S. and Rosen,B.P. (1986) Nucleotide sequence of the structural genes for an anion pump. The plasmid-encoded arsenical resistance operon. *J. Biol. Chem.*, **261**, 15030–15038.

Collaborative Computational Project Number 4 (1994) The CCP4 suite: programs for protein crystallography. *Acta Crystallogr. D*, **50**, 760–763.

Dey,S. and Rosen,B.P. (1995) Mechanisms of drug transport in prokaryotes and eukaryotes. In Georgopapadakou,N.H. (ed.), *Drug Transport in Antimicrobial and Anticancer Chemotherapy*. Dekker, New York, NY, pp. 103–132.

Dey,S., Ramachandra,M., Pastan,I., Gottesman,M.M. and Ambudkar, S.V. (1998) Photoaffinity labeling of human P-glycoprotein: effect of modulator interaction and ATP hydrolysis on substrate binding. *Methods Enzymol.*, **292**, 318–328.

Esnouf,R.M. (1997) An extensively modified version of MolScript that includes greatly enhanced coloring capabilities. *J. Mol. Graph. Model.*, **15**, 112–113, 132–134.

Georgiadis,M.M., Komiya,H., Chakrabarti,P., Woo,D., Kornuc,J.J. and

Rees,D.C. (1992) Crystallographic structure of the nitrogenase iron protein from *Azotobacter vinelandii*. *Science*, **257**, 1653–1659.
Gottesman,M.M., Pastan,I. and Ambudkar,S.V. (1996) P-glycoprotein and multidrug resistance. *Curr. Opin. Genet. Dev.*, **6**, 610–617.
Harmark,K., Anborgh,P.H., Merola,M., Clark,B.F. and Parmeggiani,A. (1992) Substitution of aspartic acid-80, a residue involved in coordination of magnesium, weakens the GTP binding and strongly enhances the GTPase of the G domain of elongation factor Tu. *Biochemistry*, **31**, 7367–7372.
Hrycyna,C.A., Ramachandra,M., Germann,U.A., Cheng,P.W., Pastan,I. and Gottesman,M.M. (1999) Both ATP sites of human P-glycoprotein are essential but not symmetric. *Biochemistry*, **38**, 13887–13899.
Hsu,C.M. and Rosen,B.P. (1989) Characterization of the catalytic subunit of an anion pump. *J. Biol. Chem.*, **264**, 17349–17354.
Hung,L.W., Wang,I.X., Nikaido,K., Liu,P.Q., Ames,G.F. and Kim,S.H. (1998) Crystal structure of the ATP-binding subunit of an ABC transporter. *Nature*, **396**, 703–707.
Jones,T.A., Zou,J.Y., Cowan,S.W. and Kjeldgaard,M. (1991) Improved methods for binding protein models in electron density maps and the location of errors in these models. *Acta Crystallogr. A*, **47**, 110–119.
Karkaria,C.E., Chen,C.M. and Rosen,B.P. (1990) Mutagenesis of a nucleotide-binding site of an anion-translocating ATPase. *J. Biol. Chem.*, **265**, 7832–7836.
Kaur,P. (1999) The anion-stimulated ATPase ArsA shows unisite and multisite catalytic activity. *J. Biol. Chem.*, **274**, 25849–25854.
Kaur,P. and Rosen,B.P. (1993) Complementation between nucleotide binding domains in an anion-translocating ATPase. *J. Bacteriol.*, **175**, 351–357.
Koonin,E.V. (1993) A superfamily of ATPases with diverse functions containing either classical or deviant ATP-binding motif. *J. Mol. Biol.*, **229**, 1165–1174.
Kraulis,P.J. (1991) MOLSCRIPT: a program to produce both detailed and schematic plots of protein structures. *J. Appl. Crystallogr.*, **24**, 946–950.
Larsen,T.M., Benning,M.M., Rayment,I. and Reed,G.H. (1998) Structure of the bis(Mg^{2+})-ATP–oxalate complex of the rabbit muscle pyruvate kinase at 2.1 Å resolution: ATP binding over a barrel. *Biochemistry*, **37**, 6247–6255.
Li,J. and Rosen,B.P. (2000) The linker peptide of the ArsA ATPase. *Mol. Microbiol.*, **35**, 361–367.
Merritt,E.A. and Murphy,M.E.P. (1994) Raster3D version 2.0. A program for photorealistic molecular graphics. *Acta Crystallogr. D*, **50**, 869–873.
Nichols,A., Sharp,K.A. and Honig,B. (1991) Protein folding and association: insights from the interfacial and thermodynamic properties of hydrocarbons. *Proteins*, **11**, 281–296.
Otwinowski,Z. and Minor,W. (1997) Processing of X-ray diffraction data collected in oscillation mode. *Methods Enzymol.*, **276**, 307–326.
Rosen,B.P. (1999) Families of arsenic transporters. *Trends Microbiol.*, **7**, 207–212.
Rosen,B.P., Bhattacharjee,H., Zhou,T. and Walmsley,A.R. (1999) Mechanism of the ArsA ATPase. *Biochim. Biophys. Acta*, **1461**, 207–215.
Schindelin,H., Kisker,C., Schlessman,J.L., Howard,J.B. and Rees,D.C. (1997) Structure of ADP × AIF4(–)-stabilized nitrogenase complex and its implications for signal transduction. *Nature*, **387**, 370–376.
Schlessman,J.L., Woo,D., Joshua-Tor,L., Howard,J.B. and Rees,D.C. (1998) Conformational variability in structures of the nitrogenase iron proteins from *Azotobacter vinelandii* and *Clostridium pasteurianum*. *J. Mol. Biol.*, **280**, 669–685.
Senior,A.E., Gros,P. and Urbatsch,I.L. (1998) Residues in P-glycoprotein catalytic sites that react with the inhibitor 7-chloro-4-nitrobenzo-2-oxa-1,3-diazole. *Arch. Biochem. Biophys.*, **357**, 121–125.
Silver,S., Budd,K., Leahy,K.M., Shaw,W.V., Hammond,D., Novick, R.P., Willsky,G.R., Malamy,M.H. and Rosenberg,H. (1981) Inducible plasmid-determined resistance to arsenate, arsenite and antimony (III) in *Escherichia coli* and *Staphylococcus aureus*. *J. Bacteriol.*, **146**, 983–996.
Sprang,S.R. (1997) G protein mechanisms: insights from structural analysis. *Annu. Rev. Biochem.*, **66**, 639–678.
Terwilliger,T.C. and Berendzen,J. (1999) Automated MAD and MIR structure solution. *Acta Crystallogr. D*, **55**, 849–861.
van den Akker,F. and Hol,W.G. (1999) Difference density quality (DDQ): a method to assess the global and local correctness of macromolecular crystal structures. *Acta Crystallogr. D*, **55**, 206–218.
Walker,J.E., Saraste,M., Runswick,M.J. and Gay,N.J. (1982) Distantly related sequences in the α- and β-subunits of ATP synthase, myosin, kinases and other ATP-requiring enzymes and a common nucleotide binding fold. *EMBO J.*, **1**, 945–951.
Weber,J., Hammond,S.T., Wilke-Mounts,S. and Senior,A.E. (1998) Mg^{2+} coordination in catalytic sites of F1-ATPase. *Biochemistry*, **37**, 608–614.
Zhou,T. and Rosen,B.P. (1997) Tryptophan fluorescence reports nucleotide-induced conformational changes in a domain of the ArsA ATPase. *J. Biol. Chem.*, **272**, 19731–19737.
Zhou,T.Q. and Rosen,B.P. (1999) Asp45 is a Mg^{2+} ligand in the ArsA ATPase. *J. Biol. Chem.*, **274**, 13854–13858.
Zhou,T., Rosen,B.P. and Gatti,D.L. (1999) Crystallization and preliminary X-ray analysis of the catalytic subunit of the ATP-dependent arsenite pump encoded by the *Escherichia coli* plasmid R773. *Acta Crystallogr. D*, **55**, 921–924.

Received May 11, 2000; revised July 6, 2000; accepted July 7, 2000